Materials and Design 186 (2020) 108266

Contents lists available at ScienceDirect

Materials and Design

journal homepage: www.elsevier.com/locate/matdes

An experimental study of anisotropic fatigue behavior of rolled AZ31B magnesium alloy

Yuqian Wang, Duke Culbertson, Yanyao Jiang *

Department of Mechanical Engineering, University of Nevada, Reno, Reno, NV, 89557, USA

HIGHLIGHTS

- Comprehensive experimental results of cyclic deformation and fatigue of a rolled Mg alloy.
- Material orientation effect on static properties of a rolled Mg alloy.
- Material orientation effect on fatigue properties of a rolled Mg alloy.
- Characteristic deformation associated with the kink points in the strain-life fatigue curve.
- Unique deformation characteristics of the 45-degree material orientation.

GRAPHICAL ABSTRACT

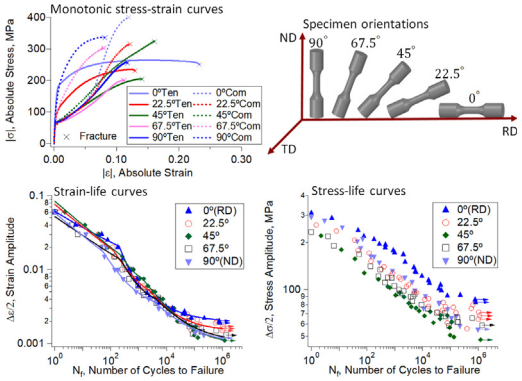

ARTICLE INFO

Article history:
Received 1 August 2019
Received in revised form 7 October 2019
Accepted 9 October 2019
Available online 15 October 2019

Keywords:
Magnesium alloy
Material orientation
Cyclic deformation
Fatigue
Anisotropy

ABSTRACT

Material orientation effects on cyclic deformation and fatigue of a rolled AZ31B magnesium (Mg) alloy were experimentally studied. Monotonic tension, monotonic compression, and fully reversed strain-controlled tension-compression experiments were conducted using testing specimens taken from a rolled plate along five different directions with respect to the rolled direction (RD): 0 °(RD), 22.5 °, 45 °, 67.5 °, and 90 °(ND). Fatigue lives range from few loading cycles to over 10^6 cycles. Significant anisotropy was observed in the monotonic and cyclic deformation behavior. Cyclic hardening was observed for all five orientations at a high strain amplitude. The strain-life curves of all the material orientations form a relatively narrow band. The strain-life curve obtained from each material orientation is characterized with two distinct kink points which are closely associated with the dominating plastic deformation mechanisms, fatigue properties, and fatigue cracking behavior. The RD specimens show the highest fatigue strength while the 45 ° specimens display the lowest fatigue strength among the five material orientations. A discussion is made on the unique deformation behavior of the 45 ° specimens.

© 2019 The Authors. Published by Elsevier Ltd. This is an open access article under the CC BY-NC-ND license (http://creativecommons.org/licenses/by-nc-nd/4.0/).

1. Introduction

Most structural components in mechanical engineering, particularly these bearing fatigue loading and at an elevated temperature, are metals. Magnesium (Mg) alloys are the lightest metallic materials that could be widely applied to load-bearing components due to their high

* Corresponding author.
E-mail address: yjiang@unr.edu (Y. Jiang).

https://doi.org/10.1016/j.matdes.2019.108266
0264-1275/© 2019 The Authors. Published by Elsevier Ltd. This is an open access article under the CC BY-NC-ND license (http://creativecommons.org/licenses/by-nc-nd/4.0/).

specific strength and specific stiffness. Fatigue is the major design concern for a structural component. Due to its hexagonal close packed (HCP) crystal structure, twinning is an important mechanism accommodating plastic deformation in Mg alloys in addition to dislocation slips [1]. Wrought (rolled, extruded, and forged) Mg alloys have advantages over the casting counterparts due to the casting defect-free conditions and their superior mechanical properties [2]. The rolling, extrusion, and forging processes result in a textured material which leads to significant anisotropic mechanical behavior [3].

In addition to initial microstructure, loading magnitude plays an important role on the plastic deformation mechanism of Mg alloys. The polar nature of twinning results in the characteristic asymmetric tension-compression deformation observed in a textured Mg alloy. Earlier studies suggested that the strain-life fatigue curve of a wrought Mg alloy exhibited a smooth transition from the low cycle fatigue (LCF) regime to the high cycle fatigue (HCF) regime [4–9]. Matsuzuki and Horibe [10] observed that the fatigue data of an extruded AZ31 alloy exhibited a bilinear tendency in the Manson–Coffin curve, suggesting twinning–detwinning dominated plastic deformation at higher strain amplitudes and dislocation slip dominated plastic deformation at lower strain amplitudes. Recent studies on several Mg alloys indicate that there exist two distinguishable kink points in the strain-life fatigue curve from the ultra-low cycle fatigue regime to the HCF regime [11,12]. These kink points divide the strain-life curve into three regimes with each regime being associated with a different degree of influence of twinning-detwinning deformation on fatigue [11]. When the strain amplitude is below the lower kink point, no persistent twinning-detwinning occurs during fatigue loading, and fatigue is exclusively due to dislocation slips. When the strain amplitude is above the lower kink point, sustainable twinning-detwinning occurs during the entire cyclic loading history. Detectable kink points in the fatigue curves were also found in extruded Mg alloys under combined axial-torsion loading with stress state influencing twinning-detwinning deformation and fatigue [13].

The mechanical properties of wrought Mg alloys are anisotropic [14–18] and the loading direction with respect to the material orientation has a significant effect on the fatigue properties [15,16,18–36]. There are still limited experimental results with respect to the material orientation effect and some reported results are even inconsistent. For rolled Mg alloys under fully reversed strain-controlled conditions, the strain-life fatigue curve obtained from loading in the rolled direction (RD) was found to be slightly higher than that tested in the thickness/normal direction (ND) [16,19]. From different studies, the strain-life curve of the ND specimens was found to be higher than that of the RD specimens of a rolled AZ31B Mg alloy in the LCF regime [20,21]. Lv et al. [15,23] conducted experiments with samples taken from a rolled AZ31B Mg sheet. It was reported that the strain-life and the stress-life curves of the transverse direction (TD) were slightly higher than those of the RD. For another rolled Mg alloy, WE43-T5, the strain-life curves were similar for the TD and RD in the LCF regime [24]. Testing specimens taken from an AM30 Mg extrusion were subjected to fully reversed strain-controlled loading in the extrusion direction (ED) and the TD [25]. The strain-life curves of the TD and the ED were found to be similar in the LCF regime. For an extruded AZ61 [26] and an extruded ZK60 [27], the strain-life curve of the ED was slightly higher than that of the TD.

The existing experimental studies of the material orientation effect on the fatigue of Mg alloys are mainly based on two or three material orientations such as RD, TD, and ND for rolled Mg alloys [15,16,18–21,23,24,28–30,37,38], and ED and TD for extruded Mg alloys [17,18,22,25–27]. Limited number of specimens were used for each material orientation with a narrow range of fatigue lives. The current work experimentally studies the effect of material orientation on the cyclic deformation and fatigue of a rolled AZ31B Mg alloy with testing specimens taken from a rolled Mg plate in five different orientations: 0°(RD), 22.5°, 45°, 67.5°, 90°(ND). The fatigue lives range from few loading cycles to over 10^6 cycles. Monotonic mechanical properties, cyclic stress-strain response, and early cracking behavior are studied. The current work aims to experimentally characterize the material orientation effect on the static and fatigue properties of a lightweight metal. The comprehensive study of the anisotropic fatigue behavior of a rolled Mg alloy offers new insights on the design and development of Mg alloys towards enhanced fatigue performance.

2. Material and experiments

2.1. Material and specimens

The material used in the study is a rolled AZ31B (Mg–3Al–1Zn) Mg alloy without heat treatment. The testing specimens were machined from a rolled plate with a thickness of 76.2 mm (Fig. 1(a)). The rolled direction, normal direction (thickness direction), and transverse direction are referred to as RD (0°), ND (90°), and TD, respectively. The initial microstructure of the material was revealed by electron backscatter diffraction (EBSD) and is shown in Fig. 1(b). The Mg alloy consists of mostly equiaxed grains with an average grain size of approximately 50 μm. The material displays a strong texture with the c-axes of most grains aligning parallel to the ND. No twins were detected in the initial microstructure.

Solid cylindrical specimens with a diameter of 8.0 mm within a gage length of 14 mm were prepared from the rolled plate with the loading axes along $\theta = 0^\circ$(RD), 22.5°, 45°, 67.5°, and 90°(ND) with respect to the RD (refer to Fig. 1(a)). Prior to an experiment, the surface within the gage section of the testing specimen was polished by using silicon carbide papers with grit No. ranging from P400 up to P1200. For

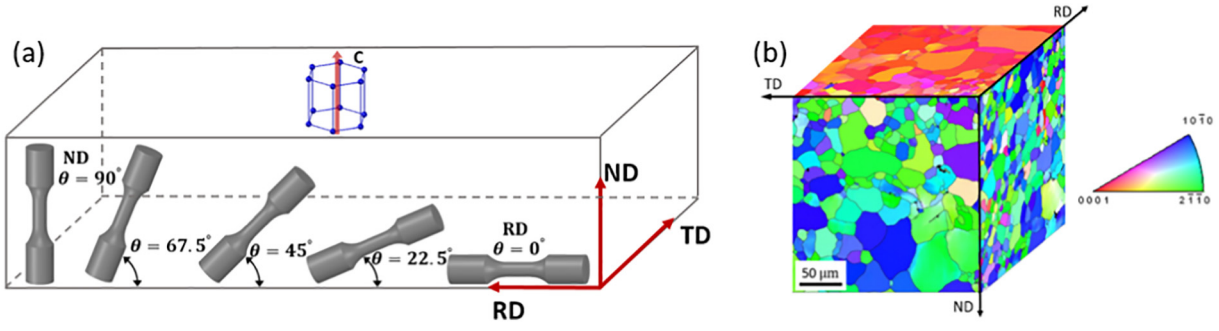

Fig. 1. Rolled AZ31B magnesium plate: (a) Specimen orientations in the rolled plate, and (b) three-dimensional stereograph of the original microstructure.

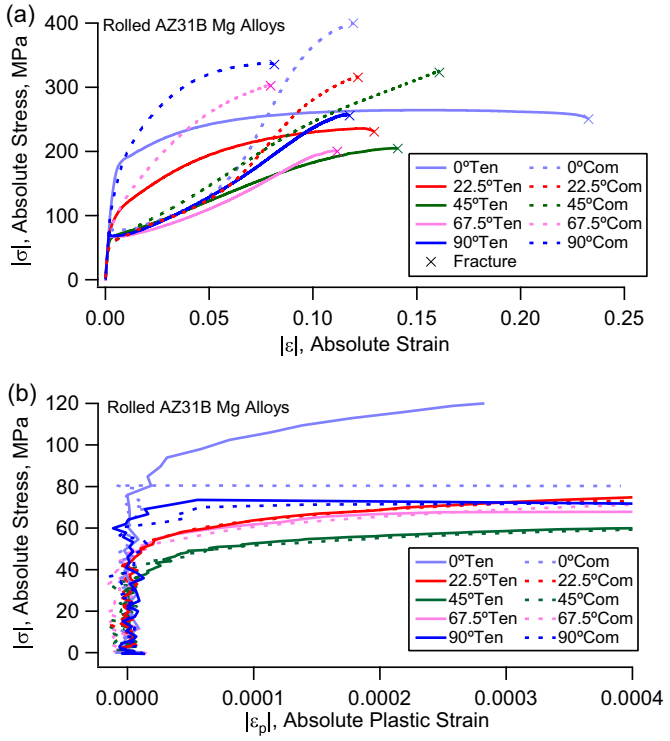

Fig. 2. Stress-strain curves of rolled AZ31B Mg alloy under monotonic tension and monotonic compression for five material orientations: (a) engineering stress-engineering strain curves, and (b) stress-plastic strain curves.

monotonic compression and very low cycle fatigue experiments, specimens with a larger diameter of 10 mm were used to avoid buckling.

2.2. Experiments

All the monotonic and cyclic loading experiments were conducted using a servo-hydraulic fatigue material testing machine in ambient. Monotonic tension and monotonic compression experiments were conducted at an approximate strain rate of $8 \times 10^{-4} s^{-1}$ to determine the static material properties of the material. Fully reversed strain-controlled tension-compression ($R_\varepsilon = -1$) fatigue experiments were conducted employing a sinusoidal waveform with strain amplitudes ranging from 0.12% to 6.00%. Loading frequencies ranged from 0.03 Hz to 15 Hz depending on the loading amplitude. The strain was measured by a clip-on extensometer. The reported fatigue life was corresponding to the moment when the stress amplitude in a loading cycle dropped by 5% from its peak value.

3. Results and discussion

3.1. Static properties

The stress-strain curves under monotonic tension and monotonic compression of the five different orientation specimens are shown in Fig. 2 and the static material properties are summarized in Table 1. Engineering stress and engineering strain are used in Fig. 2. The true fracture stresses reported in Table 1 are true stresses considering the change of cross section of the testing specimen at fracture. The stress-plastic strain curves shown in Fig. 2 (b) with small deformation are used to discuss micro-yielding of the material. To facilitate a comparison, absolute values of the stresses and the strains are used in the stress-strain curves under monotonic compression in Fig. 2.

The elasticity moduli are similar in the 0°, 22.5°, and 45° directions, and the values are slightly higher in the other two material orientations. Knowing that the rolled Mg plate has most c-axes of the grains parallel to the ND, the elasticity modulus results are consistent with the theoretical values of a single crystal Mg where the elasticity modulus along the c-axis is higher than that along a direction perpendicular to the c-axis [39,40].

Basal slips are often activated earlier than twinning due to the low critical resolved shear stress. As a result, the symmetrical nature of slips leads to the identical elastic limit under tension and under compression for a given material orientation (Fig. 2(b)). Approximating the rolled plate as a single crystal with its c-axis along the ND, the Schmid factor for basal slips is the largest for the 45° material orientation and, consequently, the elastic limit is the lowest in the 45° orientation. Basal slips in the RD and ND specimens are due to the mis-orientation of some grains of the polycrystalline Mg alloy from the perfect c-axis alignment along the ND.

The shape of the stress-strain curve under monotonic loading is associated with the deformation mechanisms. Due to the strong texture, compression in the RD (0°) and tension in the ND (90°) result in twinning, which leads to the typical sigmodal shaped stress-strain curve. When the material orientation angle θ is less than 45°, compression results in twinning and dislocation slips dominate plastic deformation under tension. As a result, the shape of the stress-strain curves are similar to these of the RD. When θ is larger than 45°, tension results in twinning and dislocation slips dominate plastic deformation under compression. For the $\theta = 45^\circ$ material orientation, the stress-strain curve under tension is similar to that under compression, signifying limited twinning.

Material strength as measured by the ultimate strength and the true fracture stress exhibits a consistent trend. The ultimate strength and the true fracture stress of the material at a given orientation is larger in compression than these under tension. With respect to the material orientation effect, the true fracture stress, which is based on true stress, is the highest in the RD (0°) followed by ND (90°), 22.5°, 45°, and 67.5°. The order is slightly different in terms of the ultimate strength which is based on the nominal or engineering stress.

The 0.2% offset yield stress is a strong function of material orientation and the dominating plastic deformation mechanism. When θ is less than 45°, the 0.2% offset yield stress is determined by basal slips when subjected to tension loading and it is dictated by twinning under compression. The opposite holds true for θ larger than 45°. Consequently, the 0.2% offset yield stress under tension continuously decreases asymptotically with increasing θ with little influence of material orientation effect after $\theta N 45^\circ$. The yield stress under compression has an opposite tendency with respect to the material orientation: the value of the yield stress under compression is similar when $\theta b 45^\circ$, and it increases significantly when θ increases from 45° to 90°.

No necking was observed in any of the monotonic tension experiments. Ductility measures in terms of either the elongation or the reduction in area (RA) provide a similar conclusion with regard to the influence of material orientation on ductility. Overall, the RD has the highest ductility and the ND and 67.5° have the lowest. The 22.5° and 45° orientations have similar ductility that falls between these of the RD and ND. Tension-compression asymmetry is observed for the elongations. Except 45° orientation, the elongation under tension is higher than that under compression. The current results are consistent in general tendency with those obtained in earlier studies [16,19].

Table 1
Static material properties of AZ31B Mg alloy.

Material Orientation	0° (RD)	22.5°	45°	67.5°	90° (ND)
Elasticity modulus, E (GPa)	44.3	44.2	44.3	46.4	47.5
Elastic limit under tension, $\sigma_e t$ (MPa)	79.1	39.1	31.8	41.9	57.6
Elastic limit under compression, $\sigma_e c$ (MPa)	79.9	40.2	31.9	41.6	57.0
0.2% offset yield stress in tension, $\sigma_y t$ (MPa)	162.5	92.3	67.3	65.8	67.9
0.2% offset yield stress in compression, $\sigma_y c$ (MPa)	78.0	74.3	69.6	87.1	141.5
Ultimate strength under tension, $S_u t$ (MPa)	264.3	235.8	200.6	195.7	257.1
Ultimate strength under compression, $S_u c$ (MPa)	415.2	315.4	325.0	307.6	337.1
True fracture stress under tension, $\sigma_f t$ (MPa)	318.9	265.6	234.1	223.1	282.9
True fracture stress under compression, $\sigma_f c$ (MPa)	350.2	278.8	275.5	282.9	311.9
Elongation under tension, $e_f t$	0.233	0.132	0.141	0.113	0.100
Elongation under compression, $e_f c$	0.130	0.122	0.160	0.087	0.085
Reduction in area under tension, RA (%)	15.1	12.2	12.7	8.6	9.6

3.2. Fatigue results and kink points

Fully reversed strain-controlled tension-compression fatigue experiments in the five material orientations are summarized in Appendix A (Tables A1-A5). The stress amplitudes and the mean stresses were taken at approximate half fatigue lives. The plastic strain energy density per loading cycle, ΔW^p, was calculated from the stress-strain hysteresis loop at approximate half fatigue life.

The strain-life fatigue curves are shown in Fig. 3. An arrow after a data point denotes an experiment without fatigue failure after more than 10^6 loading cycles. The stress-life fatigue curves of the five material orientations are shown in Fig. 4.

The strain-life fatigue curves of most metallic materials under fully reversed strain-controlled tension-compression loading can be described by the following three-parameter equation,

$$\left(\frac{\Delta\varepsilon}{2}-\varepsilon_0\right)^{\xi} N_f = C \tag{1}$$

where $\Delta\varepsilon/2$ is the strain amplitude, N_f is the number of loading cycles to failure, and ε_0, ξ, and C are the constants determined by fitting the experimental data. If a strain-life curve needs more than one such an equation to describe, the intersection of two curves forms a kink point. For the Mg alloys, three equations are needed to describe the whole strain-life curve with fatigue life ranging from a few loading cycles to over a million loading cycles. As a result, there are two kink points in each strain-life curve. In Fig. 3, the kink points are denoted by black solid circles. The stress amplitudes, strain amplitudes, and fatigue lives corresponding to the kink points of all the five material orientations are summarized in Table 2.

The kink points in a strain-life curve reflect the demarcation of dominating cyclic plastic deformation mechanisms. Earlier investigations on extruded Mg alloys tested in the extrusion direction reveal that kink points exist in the strain-life curves that demarcate the influence of twinning-detwinning deformation on fatigue [11,12,41]. The current study further suggests that two kink points exist in the strain-life fatigue curve of any given material orientation. Consistent with the previous observations, the lower kink point signifies the involvement of persistent twinning-detwinning deformation during fatigue loading. When the strain amplitude is lower than the lower kink point, stabilized cyclic plastic

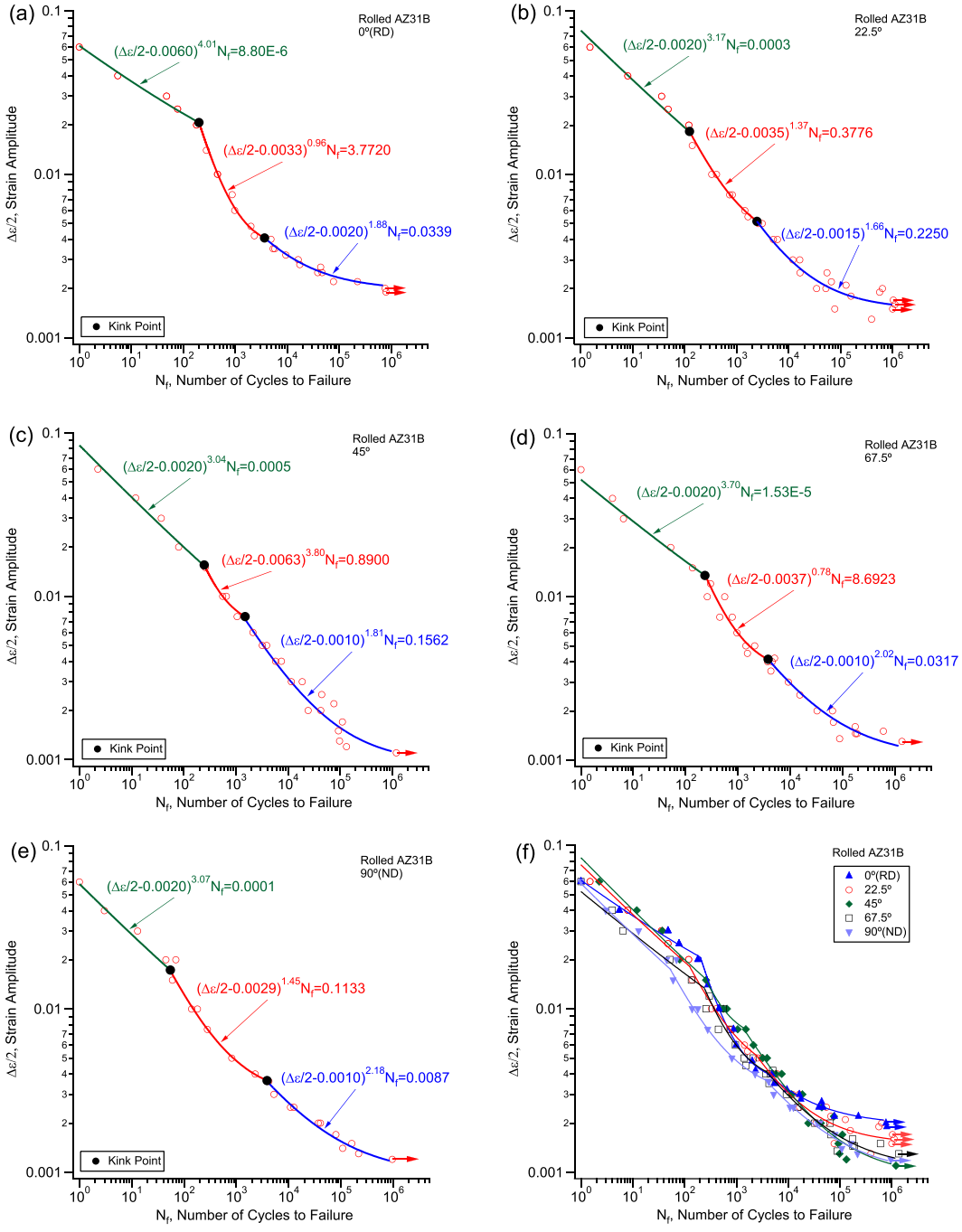

Fig. 3. Strain-life curves under fully reversed strain-controlled tension-compression for rolled AZ31B alloys: (a) 0 °(RD), (b) 22.5 °, (c) 45 °, (d) 67.5 °, (e) 90 °(ND), and (f) all orientations.

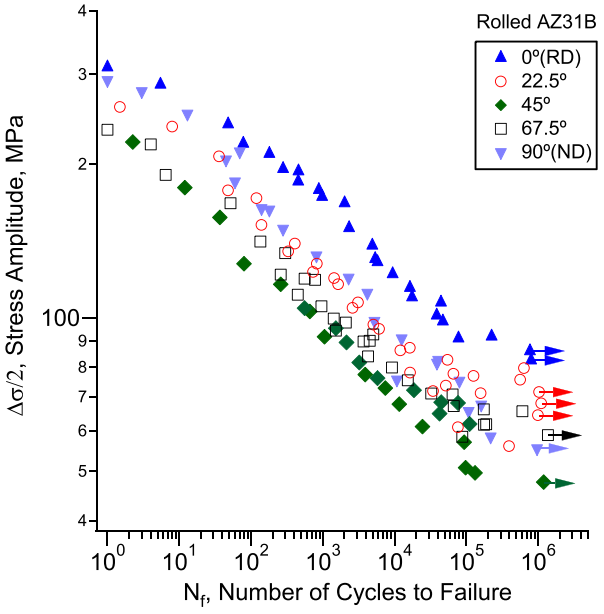

Fig. 4. Stress-life curves for rolled AZ31B magnesium alloys.

deformation is due to basal slips without involving twinning-detwinning, and the stress-strain hysteresis loops are symmetric. The influence of twins and twinning on fatigue is minimal. When the strain amplitude is higher than the lower kink point, twinning-detwinning occurs during cyclic loading. One or both upper and lower branches of the stress-strain hysteresis loop shows a sigmodal shape. Twinning occurs under either tension or compression, and detwinning occurs in the reversed loading reversal. The sigmodal shape is characterized with an inflection point which often reflects completion of twinning or detwinning and start of non-basal slip during a loading reversal.

A loading amplitude higher than the upper kink point in a strain-life curve results in sustainable non-basal slips in both loading and reversed loading reversals, which will be discussed in detail in the next section. Results in Fig. 3 indicate that the strain-lives above the upper kink point show an approximately linear relationship in log-log scale.

When all the strain-life curves of the five material orientations are plotted together (Fig. 3(f)), the features with the kink points are lost but the presentation leads to an overall observation: all the strain-life curves fall in a relatively narrow band. The anisotropic fatigue properties are better reflected in the stress-life curves shown in Fig. 4. A glance of the results reveals that the RD material orientation has the highest stress-life curve and the 45 ° orientation has the lowest, with the results of the other three material orientations falling in between. Both the stress-life curves and the strain-life curves show that the fatigue lives in the RD are longer than those in the ND at a given strain amplitude or stress amplitude. The fatigue results in the RD and ND in the current work are consistent with these reported earlier on a similar material [16,19]. However, a different tendency was reported by other researchers [20,21] on a similar rolled Mg alloy.

For all the specimens with different material orientations, fatigue cracks were initiated from the outer specimen surface, and the process was followed by crack propagation into the interior of the specimen till total fracture. The overall fatigue cracking behavior is related to the upper kink point for all the five material orientations and is irrelevant to the loading direction with respect to the material orientation. When the strain amplitude is lower than the upper kink point, early cracking was found to form on the material plane perpendicular to the axial loading direction for specimens of all material orientations. An example is shown in Fig. 5(a) for an ND specimen loaded at a strain amplitude of 0.13%. When the strain amplitude is above the upper kink point, which corresponding to very low fatigue lives, the fatigue cracking surface is either a serrated surface profile (Fig. 5(b)) or approximately 45° from the loading axis (Fig. 5(c)) for all the material orientations. The observations suggest that the fatigue cracking behavior under tension-compression loading is associated with the strain amplitude only and is independent of the direction of the loading with respect to the original texture of the material.

3.3. Cyclic stress-strain response

The characteristic kink points in the strain-life fatigue curves are closely associated with the cyclic plastic deformation of the material. Fig. 6 shows the stress-strain hysteresis loops of selective strain amplitudes at approximate half-fatigue lives under fully reversed strain-controlled tension-compression fatigue experiments of the five material orientations. A solid circle on a stress-strain hysteresis loop denotes an inflection point which mathematically is the point where the second derivative of the stress with respect to the strain is zero. The inflection points reflect the transition of two dominating plastic deformation mechanisms: from twinning or detwinning to non-basal slips. The shape of the stress-strain hysteresis loops is dependent on the material orientation and the applied strain amplitude.

When the strain amplitude is lower than the lower kink point, a detailed observation of the stress-strain hysteresis loops reveals that the shape is symmetrical with both the upper and lower branches of the stress-strain hysteresis loops being a concave or convex shape for all the five material orientations. No persistent twinning-detwinning occurs during fatigue loading. Such an observation is consistent with that made on extruded Mg alloys tested in the extrusion direction [11,12,14,17,26,27,41].

For the fully reversed strain-controlled loading with the strain amplitude higher than the lower kink point, the compression reversal results in twinning and the tension reversal results in detwinning when the material orientation θ is less than 45 °. When θ is larger than 45 °, twinning occurs in the tension reversal and detwinning occurs during compression reversal. When the strain amplitude is higher than the lower kink point but less than the upper kink point, the detwinning loading reversal forms a sigmodal shape while the twinning reversal results in either a concave or convex shape. In this case, a sigmodal shape contains an inflection point which is an indicator of completion of detwinning and start of non-basal slips.

For all the five material orientations when the strain amplitude is above the upper kink point, both the upper and lower branches of the stress-strain hysteresis loop exhibit a sigmodal shape and therefore, there are two inflection points in a stress-strain hysteresis loop. In addition, the shape of the hysteresis loop tends to be more symmetric as the strain amplitude increases. For the material orientation $\theta b45^{\circ}$, the compression loading reversal is characterized by twinning and non-basal slips. The inflection point in the lower branch of the hysteresis loop signifies a start of non-basal slips with continuous twinning. During the tension loading reversal, which corresponds to the upper branch of the stress-strain hysteresis loop, detwinning occurs. The inflection point reflects the completion of detwinning and start of non-basal slips. The overall phenomenon is similar to that explained earlier for extruded Mg alloys loaded in the extrusion direction [10–12,14,17,26,27,41–48]. For the material orientation $\theta N45^{\circ}$, the inflection points represent the same characteristics but twinning occurs in the tension loading reversal and detwinning occurs in the compression reversals.

The variations of the stress amplitudes and the mean stress with the number of loading cycles under fully reversed strain-controlled loading reveal the cyclic hardening behavior of the material and are shown in Fig. 7 for the five material orientations. A glance of the results suggests that noticeable cyclic hardening occurs at a strain amplitude higher than the lower kink point for any material orientation, and a higher strain amplitude results in more significant cyclic hardening. Since a strain amplitude higher than the lower kink point is associated with persistent twinning-detwinning, it can be speculated that twinning-detwinning is the main contributor to the observed cyclic hardening in a Mg alloy. Another general observation from Fig. 7 is that positive mean stresses are found in the $\theta b45^{\circ}$ material orientations and compressive mean stresses are accompanied in the $\theta N45^{\circ}$ material orientations. The $\theta = 45^{\circ}$ material orientation has virtually zero mean stresses, which is consistent with the near symmetrical stress-strain hysteresis loops of the material orientation as shown in Fig. 6(c).

The stress-strain hysteresis loops in the RD and in the ND at identical strain amplitudes are similar after 180° rotation but not identical. Similarly, the hysteresis loops in the 22.5 ° and these in the 67.5 ° at identical strain amplitudes are similar after 180° rotation but not identical. Such an observation can be further collaborated with the results of the cyclic stress-plastic strain curves shown in Fig. 8 for the five material orientations. The vertical axis in Fig. 8 represents the stress amplitude of an experiment and the horizontal axis is the plastic strain amplitude which is equal to the strain amplitude subtracting the

Table 2
Kink points for different material orientations.

Material Orientation, °	Lower Kink Point			Upper Kink Point		
	$\Delta\varepsilon/2$, %	$\Delta\sigma/2$, MPa	N_f, cycles	$\Delta\varepsilon/2$, %	$\Delta\sigma/2$, MPa	N_f, cycles
0 (RD)	0.41	144	3680	2.07	211	200
22.5	0.52	111	2460	1.83	165	120
45	0.75	95	1500	1.56	118	250
67.5	0.41	92	3770	1.35	138	230
90 (ND)	0.37	112	3870	1.73	197	50

Note: $\Delta\varepsilon/2$ strain amplitude; $\Delta\sigma/2$-stress amplitude; N_f-number of loading cycles to failure.

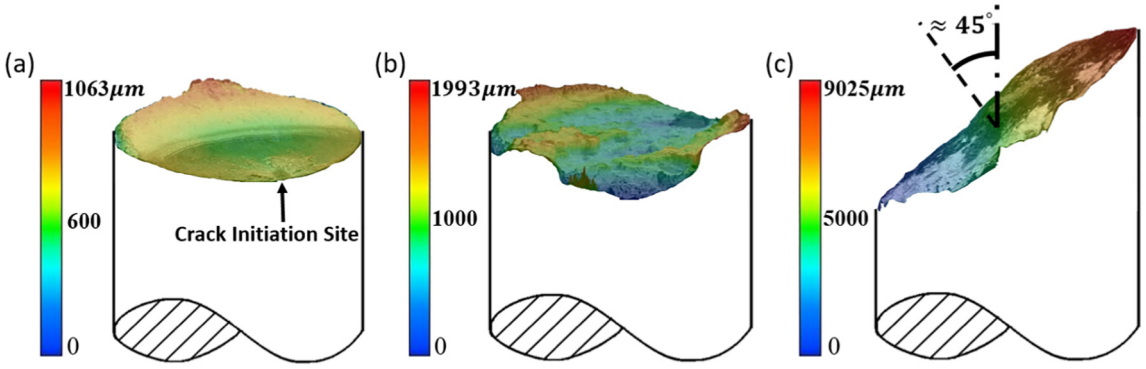

Fig. 5. Typical fracture surface after fatigue of 90° (ND) specimens: (a) $\Delta\varepsilon/2 = 0.13\%$, (b) $\Delta\varepsilon/2 = 3.00\%$, and (c) $\Delta\varepsilon/2 = 6.00\%$.

elastic strain amplitude. All the quantities are taken from the stress-strain hysteresis loop at approximately half fatigue life for each testing specimen. Overall, the RD material orientation has the highest cyclic stress-plastic strain curve and the 45° orientation yields the lowest cyclic stress-strain curve.

3.4. 45° material orientation

The results obtained from testing 45° material orientation deserve a further discussion. There are six crystallographic equivalent tension twin variants in a hexagonal close packed (HCP) Mg crystal. Associated with each variant, there is a corresponding value that correlates to the resolved shear stress of the twin plane along the twin direction. This value, called Schmid factor (SF), is often used in twin variant selection analysis [49,50]. When analyzing a grain, the largest SF among those of the six variants is used when discussing twinning. Assuming a perfect c-axis alignment in the ND of the rolled plate (refer to Fig. 1), the maximum SF of the six $10\bar{1}2$ tension twinning variants is 0.25 for the 45° orientation. While still large enough to activate twinning, this value is the smallest among the five material orientations and, as a result, twinning is more difficult to occur for the 45° material orientation. Consequently as shown in Fig. 3 and Table 2, the strain amplitude corresponding to the lower kink point in the strain-life curve is the highest among all the material orientations.

Fig. 9 shows the EBSD results after the 45° orientation specimens were loaded at a strain amplitude of 2.0% for 40 loading cycles and terminated at 2.00% and −2.00%,

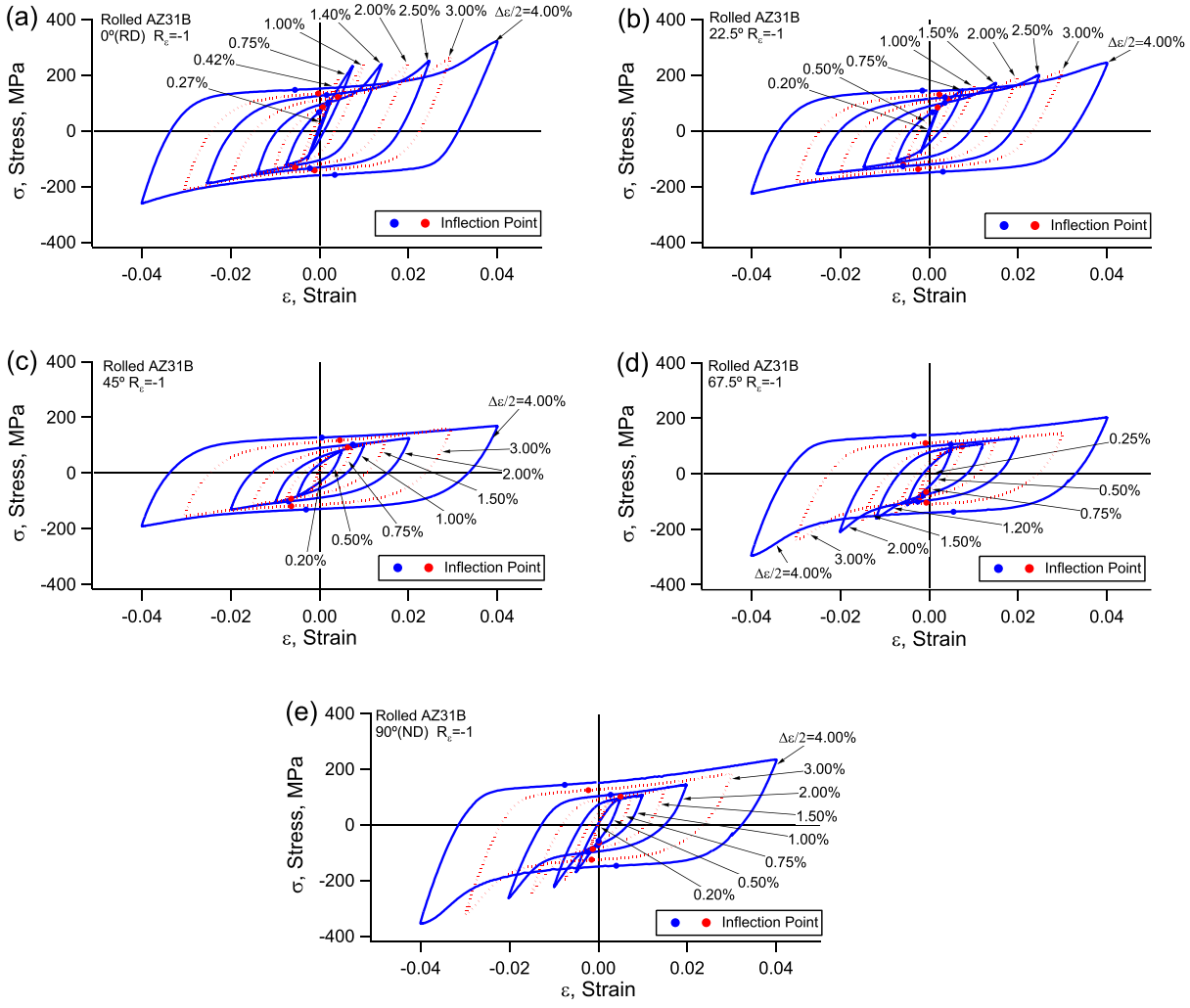

Fig. 6. Stabilized stress-strain hysteresis loops: (a) 0° (RD), (b) 22.5°, (c) 45°, (d) 67.5°, and (e) 90° (ND).

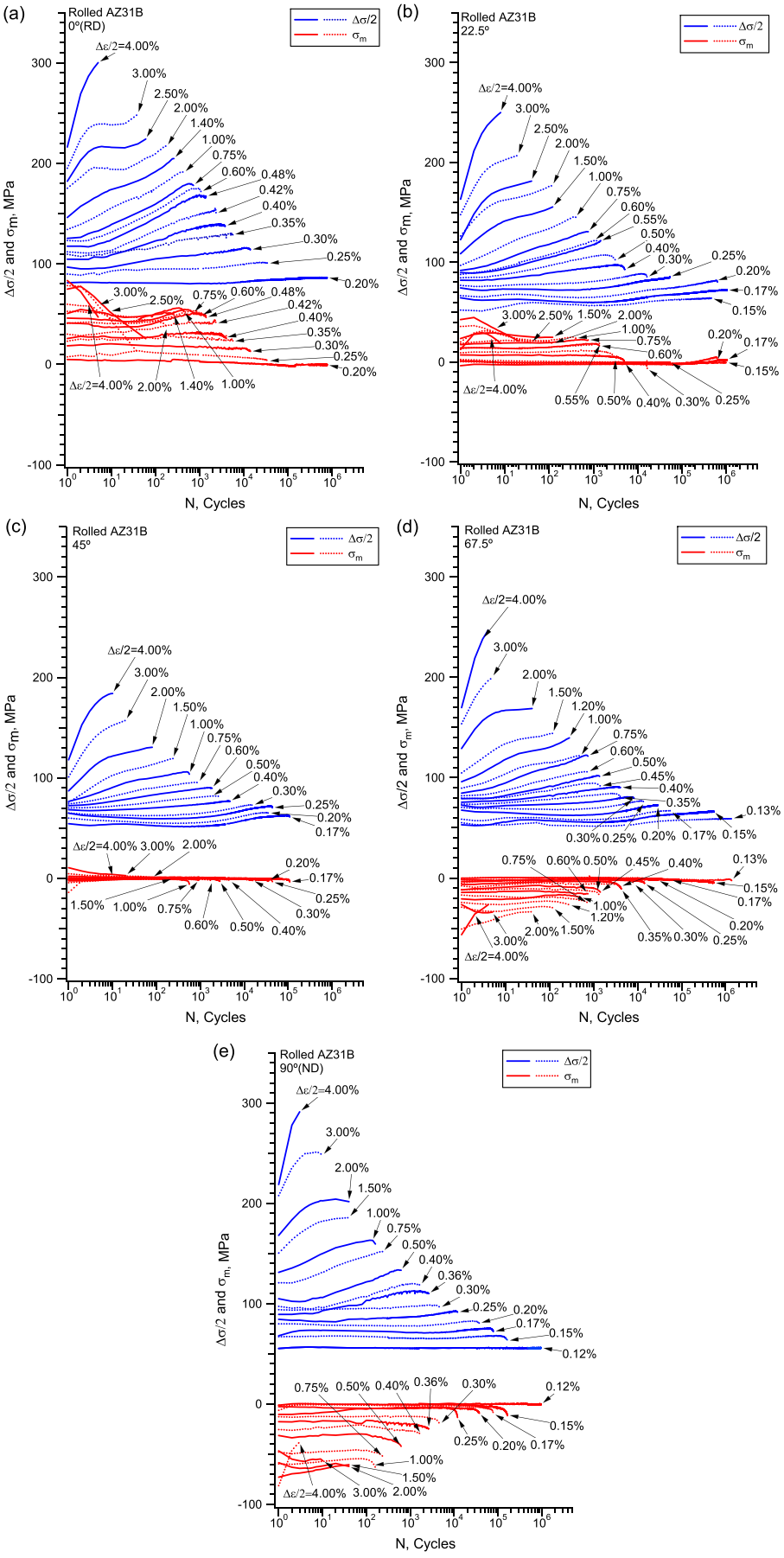

Fig. 7. Variations of stress amplitude and mean stress with the number of loading cycles: (a) 0 ° (RD), (b) 22.5 °, (c) 45 °, (d) 67.5 °, and (e) 90 ° (ND).

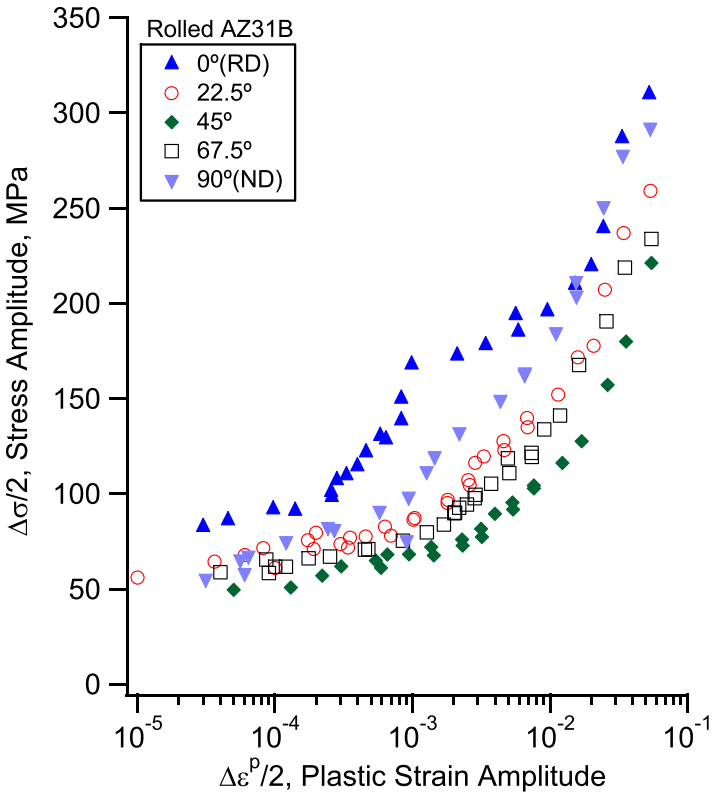

Fig. 8. Cyclic stress-plastic strain curves.

respectively, before unloading to zero stress. Accounting for the distribution of c-axes of the grains in the rolled polycrystalline Mg alloy, three grain orientation types are examined by EBSD based on their favorability to twin: grains that are favorable for twinning under compression (G_1, G_2, G_7, G_8), grains that are not favorable for twinning under both compression and tension (G_3, G_4, G_9, G_{10}), and grains that are favorable for twinning under tension (G_5, G_6, G_{11}, G_{12}). Grains favorable for twinning typically have a SF larger than 0.25 based on the statistics among approximately 70 grains examined in the observation areas shown in the EBSD inverse pole figure maps (Fig. 9). With high positive SF values, twinning occurs in G_1 and G_2 under compression. Simultaneously with the occurrence of twinning in G_1 and G_2, detwinning is expected to occur in G_5 and G_6. This is because twinning is very likely to have occurred in G_5 and G_6 during the previous tension loading reversal due to their high SF values. In G_5, a few residual twins are visible, and the twins formed during tensile loading in G_6 are expected to have been completely detwinned at the end of the compression reversal. No twinning-detwinning occurs in G_3 and G_4. Similar observations can be made from the results terminated at 2.00% (tension) after 40 loading cycles. G_{11} and G_{12}, due to large positive SF values, experience twinning under tensile loading, and during the same tensile loading reversal, detwinning occurs in G_7 and G_8. An analysis of the twin in G_8 indicates that it is a residual twin formed during previous compression loading. No twinning or detwinning occurs in G_9 and G_{10} during the entire loading cycle due to the small SF values.

To summarize, there are several major differences in terms of twinning and detwinning between the $\theta = 45^\circ$ specimens and the specimens of other material orientations. Due to smaller SF, twinning is more difficult to occur in the $\theta = 45^\circ$ specimens than the specimens of other material orientations. Consequently, the strain amplitude corresponding to the lower kink point in the strain-life fatigue curves is the highest among all material orientations. For the material orientation other than $\theta = 45^\circ$, twinning occurs in the grains with orientations favorable for twinning during a loading reversal and detwinning occurs in the same group of grains during the reversed loading reversal. With the $\theta = 45^\circ$ material orientation, twinning and detwinning occur simultaneously under both tension and compression. Twinning occurs in a group of grains oriented favorably for twinning under tension (such as G_5, G_6, G_{11} and G_{12} in Fig. 9) and simultaneously, detwinning occurs in a second group of grains oriented favorably for twinning under compression (such as G_1, G_2, G_7, and G_8 in Fig. 9). During the compression loading reversal, twinning occurs in the second group of grains and concurrently, detwinning occurs in the first group of grains. Therefore, both twinning and detwinning occur during both tension and compression loading reversals, which results in the observed symmetric stress-strain hysteresis loops under cyclic loading in 45° material orientation.

Another uniqueness of the $\theta = 45^\circ$ orientation is the less percentage of grains being twinned and detwinned during the fully reserved strain-controlled tension-compression. At a strain amplitude of 2.00% after 40 loading cycles, based on the statistics of 70 grains in the observation area shown in Fig. 9(a), approximately 30% of the total grains experience twinning, 30% of the total grains undergo detwinning, and the rest grains experience no twinning or detwinning. In contrast, for the ND specimen, approximately 90% of the grains undergo twinning at a strain of 2.0% under tension and the same group of grains experience detwinning during compression.

4. Conclusions

A comprehensive experimental study of the material orientation effect on mechanical properties of a rolled AZ31B Mg alloy was performed with monotonic tension, monotonic compression, and fully reversed strain-controlled tension-compression fatigue experiments in five material orientations with fatigue lives ranging from few loading cycles to over 10^6 cycles. The following conclusions can be drawn from the study.

1) The elastic limit under tension is identical to that under compression for any given material orientation with the highest to lowest following the order 0° (RD), 90° (ND), 67.5°, 22.5°, and 45°. The ultimate strength and true fracture strength are higher under compression than these under tension for a given material orientation. The true fracture stress and ductility are the highest in the RD (0°).
2) Overall, the strain-life fatigue curves of all the five material orientations fall in a relatively narrow band. Anisotropic fatigue properties are reflected in the stress-life curves. The RD material orientation has the highest stress-life curve and the 45° orientation has the lowest.
3) The strain-life fatigue curve of any given orientation is characterized by two kink points. The stress-strain hysteresis loop is symmetric when strain amplitude is lower than the lower kink point. When the strain amplitude is in between the upper and lower kink points, the asymmetric stress-strain hysteresis loop contains one inflection point which signifies completion of detwinning and start of non-

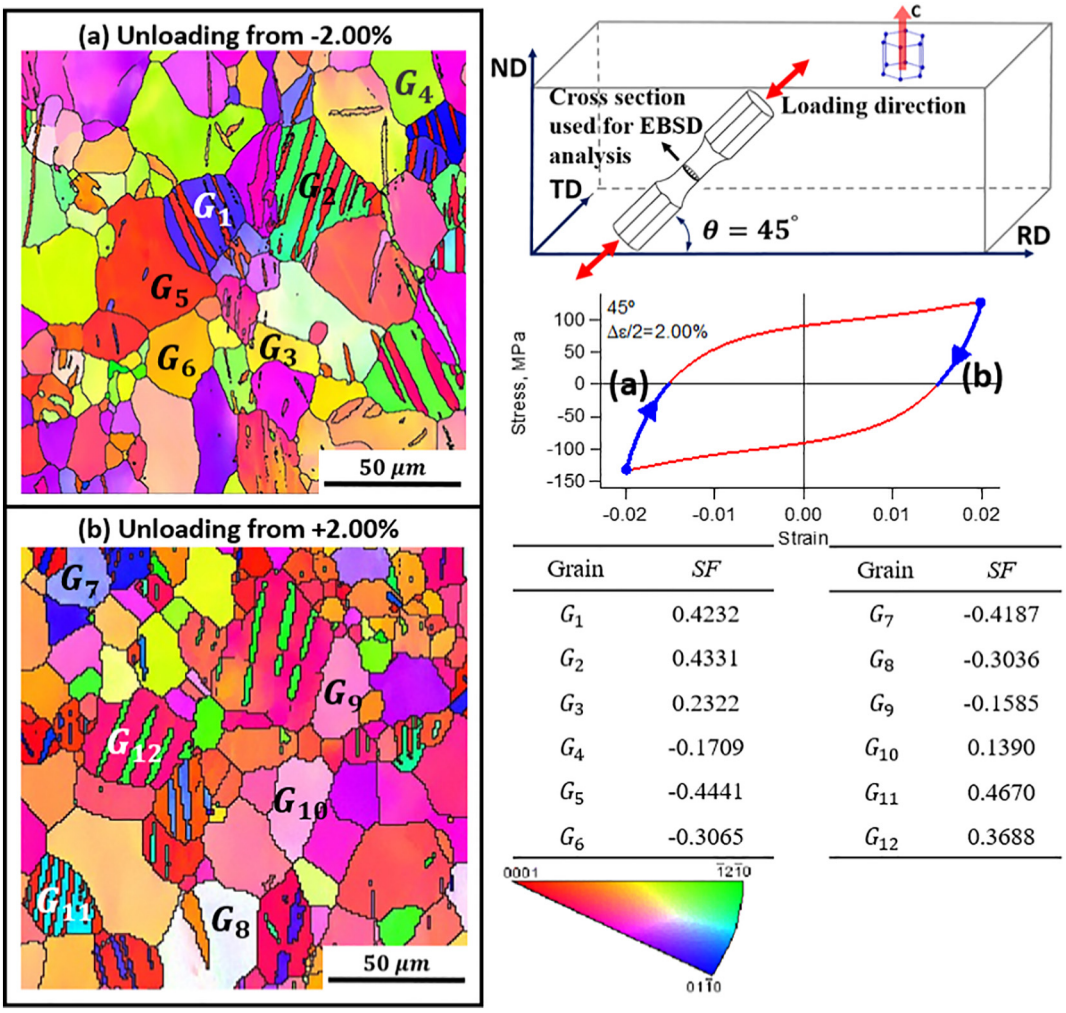

Grain	*SF*	Grain	*SF*
G_1	0.4232	G_7	-0.4187
G_2	0.4331	G_8	-0.3036
G_3	0.2322	G_9	-0.1585
G_4	-0.1709	G_{10}	0.1390
G_5	-0.4441	G_{11}	0.4670
G_6	-0.3065	G_{12}	0.3688

Fig. 9. EBSD inverse pole figure maps and maximum Schmid factors of representative grains of the 45° orientation specimen after loaded at a strain amplitude of 2.0% for 40 cycles.

basal slips. When the strain amplitude is higher than the upper kink point, the stress-strain hysteresis loop tends to be symmetric with both upper and lower branches having a sigmodal shape.

4) Cyclic hardening is proportional to the loading amplitude and is observed for all the five material orientations when the strain amplitude is higher than the lower kink point. Positive mean stresses are shown in the $\theta b45^\circ$ material orientations and compressive mean stresses are found in the $\theta N45^\circ$ material orientations. The $\theta = 45^\circ$ material orientation has virtually zero mean stresses.
5) When the strain amplitude is lower than the upper kink point, early cracking is found to form on the surface perpendicular to the specimen axis. When the strain amplitude is above the upper kink point, the fatigue cracking surface is either approximately 45 degree from the loading axis or a serrated surface profile. The observed fatigue cracking behavior is independent of the material orientation.
6) For the 45° orientation, twinning occurs in one group of grains and simultaneously detwinning occurs in another group of grains during loading and during reversed loading. The Schmid factor for twinning is statistically low in the 45° orientation specimens, thus low percentage of grains favorable for twinning, as compared with the other material orientations. Consequently, the strain amplitude corresponding to the lower kink point in the strain-life fatigue curve in the 45° material orientation is the highest among all the material orientations.

CRediT authorship contribution statement

Yuqian Wang: Data curation, Formal analysis, Writing - original draft, Writing - review & editing. **Duke Culbertson:** Formal analysis, Writing - original draft, Writing - review & editing. **Yanyao Jiang:** Data curation, Funding acquisition, Supervision, Validation, Writing - original draft, Writing - review & editing.

Declaration of competing interest

The authors declare no competing financial interest.

Acknowledgment

The research was supported by the U.S. National Science Foundation (CMMI-1762312).

Appendix A. Supplementary data

Supplementary data to this article can be found online at https://doi.org/10.1016/j.matdes.2019.108266.

Data availability

The raw/processed data required to reproduce these findings cannot be shared at this time due to technical or time limitations.

References

[1] S. Graff, W. Brocks, D. Steglich, Yielding of magnesium: from single crystal to polycrystalline aggregates, Int. J. Plast. 23 (12) (2007) 1957–1978.
[2] C. Bettles, M. Gibson, Current wrought magnesium alloys: strengths and weaknesses, JOM 57 (5) (2005) 46–49.
[3] X.Y. Lou, M. Li, R.K. Boger, S.R. Agnew, R.H. Wagoner, Hardening evolution of AZ31B Mg sheet, Int. J. Plast. 23 (1) (2007) 44–86.
[4] A.N. Chamos, S.G. Pantelakis, G.N. Haidemenopoulos, E. Kamoutsi, Tensile and fatigue behavior of wrought magnesium alloys AZ31 and AZ61, Fatigue Fract. Eng. Mater. Struct. 31 (2008) 812–821.
[5] K. Shiozawa, J. Kitajima, T. Kaminashi, T. Murai, T. Takahashi, Low-cycle fatigue deformation behavior and evaluation of fatigue life on extruded magnesium alloys, Procedia Eng 10 (2011) 1244–1249.
[6] S. Hasegawa, Y. Tsuchida, H. Yano, M. Matsui, Evaluation of low cycle fatigue life in AZ31 magnesium alloy, Int. J. Fatigue 29 (9–11) (2007) 1839–1845.
[7] C.J. Geng, B.L. Wu, X.H. Du, Y.D. Wang, Y.D. Zhang, F. Wagner, C. Esling, Low cycle fatigue behavior of the textured AZ31B magnesium alloy under the asymmetrical loading, Mater. Sci. Eng. A 560 (2013) 618–626.
[8] L. Chen, C. Wang, W. Wu, Z. Liu, G. Stoica, L. Wu, P. Liaw, Low-cycle fatigue behavior of an as-extruded AM50 magnesium alloy, Metall. Mater. Trans. A 38 (13) (2007) 2235–2241.
[9] S.H. Park, S. Hong, B.H. Lee, C.S. Lee, Fatigue life prediction of rolled AZ31 magnesium alloy using energy-based model, Int. J. Mod. Phys. B 22 (2008) 5503–5508.
[10] M. Matsuzuki, S. Horibe, Analysis of fatigue damage process in magnesium alloy AZ31, Mater. Sci. Eng. A 504 (2009) 169–174.
[11] Y. Xiong, Y. Jiang, Fatigue of ZK60 magnesium alloy under uniaxial loading, Int. J. Fatigue 64 (2014) 74–83.
[12] S. Dong, Y. Jiang, J. Dong, F. Wang, W. Ding, Cyclic deformation and fatigue of extruded ZK60 Magnesium alloy with aging effects, Mater. Sci. Eng. A 615 (2014) 262–272.
[13] F. Castro, Y. Jiang, Fatigue of extruded AZ31B magnesium alloy under stress- and strain-controlled conditions including step loading, Mech. Mater. 108 (2017) 77–86.
[14] C. Chen, T. Liu, C. Lv, L. Lu, D. Luo, Study on cyclic deformation behavior of extruded Mg–3Al–1Zn alloy, Mater. Sci. Eng. A 539 (2012) 223–229.
[15] F. Lv, F. Yang, Q.Q. Duan, Y.S. Yang, S.D. Wu, S.X. Li, Z.F. Zhang, Fatigue properties of rolled magnesium alloy (AZ31) sheet: influence of specimen orientation, Int. J. Fatigue 33 (5) (2011) 672–682.
[16] L. Wu, S.R. Agnew, Y. Ren, D.W. Brown, B. Clausen, G.M. Stoica, H.R. Wenk, P.K. Liaw, The effects of texture and extension twinning on the low-cycle fatigue behavior of a rolled magnesium alloy, AZ31B, Mater. Sci. Eng. A 527 (2010) 7057–7067.
[17] J.B. Jordon, H.R. Brown, H. El Kadiri, H.M. Kistler, R.T. Lett, J.C. Baird, A.A. Luo, Investigation of fatigue anisotropy in an extruded magnesium alloy, Int. J. Fatigue 51 (2013) 8–14.
[18] S. Ishihara, S. Taneguchi, H. Shibata, T. Goshima, A. Saiki, Anisotropy of the fatigue behavior of extruded and rolled magnesium alloys, Int. J. Fatigue 50 (2013) 94–100.
[19] Y. Xiong, Y. Jiang, Cyclic deformation and fatigue of rolled AZ80 magnesium alloy along different material orientations, Mater. Sci. Eng. A 667 (2016) 58–67.
[20] S.H. Park, S.G. Hong, W. Bang, C.S. Lee, Effect of anisotropy on the low-cycle fatigue behavior of rolled AZ31 magnesium alloy, Mater. Sci. Eng. A 527 (2010) 417–423.
[21] S.G. Hong, S.H. Park, Y.H. Huh, C.S. Lee, Anisotropy fatigue behavior of rolled Mg-2Al-1Zn alloy, J. Mater. Res. 25 (2010) 966–971.
[22] Y. Wu, R. Zhu, J. Wang, W. Ji, Role of twining and slip in cyclic deformation of extruded Mg-3%-al-1%Zn alloys, Scr. Mater. 63 (11) (2010) 1077–1080.
[23] F. Lv, F. Yang, Q.Q. Duan, T.J. Luo, Y.S. Yang, S.X. Li, Z.F. Zhang, Tensile and low-cycle fatigue properties of Mg–2.8% Al–1.1% Zn–0.4% Mn alloy along the transverse and rolling directions, Scr. Mater. 61 (9) (2009) 887–890.
[24] S. Ghorbanpour, B. McWilliams, M. Knezevic, Low-cycle fatigue behavior of rolled WE43-T5 magnesium alloy, Fatigue Fract. Eng. Mater. Struct. 42 (6) (2019) 1357–1372.
[25] A. Roostaei, H. Jahed, Role of loading direction on cyclic behavior characteristics of AM30 extrusion and its fatigue damage modelling, Mater. Sci. Eng. A 670 (2016) 26–40.
[26] J.B. Jordon, J.B. Gibson, M.F. Horstemeyer, H. El Kadiri, J.C. Baird, A.A. Luo, Effect of twinning, slip, and inclusions on the fatigue anisotropy of extrusion-textured AZ61 magnesium alloy, Mater. Sci. Eng. A 528 (2011) 6860–6871.
[27] Y. Xiong, X. Gong, Y. Jiang, Effect of initial texture on fatigue properties of extruded ZK60 magnesium alloy, Fatigue Fract. Eng. Mater. Struct. 41 (7) (2018) 1504–1513.
[28] Y.C. Lin, X.M. Chen, Z.H. Liu, J. Chen, Investigation of uniaxial low-cycle fatigue behavior of hot-rolled AZ91 magnesium alloy, Int. J. Fatigue 48 (2013) 122–132.
[29] S.H. Park, S.G. Hong, J.H. Yoon, C.S. Lee, Influence of loading direction on the anisotropic fatigue properties of rolled magnesium alloy, Int. J. Fatigue 87 (2016) 210–215.
[30] K. Hazeli, H. Askari, J. Cuadra, F. Streller, R.W. Carpick, H.M. Zbib, A. Kontsos, Microstructure-sensitive investigation of magnesium alloy fatigue, Int. J. Plast. 68 (2015) 55–76.
[31] F. Lv, Y.S. Yang, S.X. Li, Z.F. Zhang, Effects of hysteresis energy and mean stress on low-cycle fatigue behaviors of an extruded magnesium alloy, Scr. Mater. 65 (2011) 53–56.
[32] A.H. Pahlevanpour, S.M.H. Karparvarfard, S.K. Shaha, S.B. Behravesh, S. Adibnazari, H. Jahed, Anisotropy in the quasi-static and cyclic behavior of ZK60 extrusion: characterization and fatigue modeling, Mater. Des. 160 (2018) 936–948.
[33] C. Wang, T.J. Luo, J.X. Zhou, Y.S. Yang, Anisotropic cyclic deformation behavior of extruded ZA81M magnesium alloy, Int. J. Fatigue 96 (2017) 178–184.
[34] D. Hou, T. Liu, L. Luo, L. Lu, H. Chen, D. Shi, Twinning behaviors of a rolled AZ31 magnesium alloy under multidirectional loading, Mater. Char. 124 (2017) 122–128.
[35] Y. Ling, A.A. Roostaei, G. Glinka, H. Jahed, Fatigue of ZEK100-F magnesium alloy: characterisation and modelling, Int. J. Fatigue 125 (2019) 179–186.
[36] S.H. Kim, S.G. Hong, J.H. Lee, C.S. Lee, J. Yoon, H. Yu, S.H. Park, Anisotropic in-plane fatigue behavior of rolled magnesium alloy with {10-12} twins, Mater. Sci. Eng. A 700 (2017) 191–197.
[37] F.A. Mirza, K. Wang, S.D. Bhole, J. Friedman, D.L. Chen, D.R. Ni, B.L. Xiao, Z.Y. Ma, Strain-controlled low cycle fatigue properties of rare-earth containing ME20 magnesium alloy, Mater. Sci. Eng. A 661 (2016) 115–125.
[38] S.H. Park, Effect of initial twins on the stress-controlled fatigue behavior of rolled magnesium alloy, Mater. Sci. Eng. A 680 (2017) 214–220.
[39] T.R. Long, C.S. Smith, Single-crystal elastic constants of magnesium and magnesium alloys, Acta Metall. 5 (4) (1957) 200–207.
[40] G. Simmons, H. Wang, Single Crystal Elastic Constants and Calculated Aggregate Properties, second ed. MIT Press, Cambridge (MA), 1971 370.
[41] Y. Xiong, Q. Yu, Y. Jiang, Cyclic deformation and fatigue of extruded AZ31B magnesium alloy under different strain ratios, Mater. Sci. Eng. A 649 (2016) 93–103.
[42] F. Wang, M. Liu, J. Sun, M. Feng, L. Jin, J. Dong, Y. Jiang, Effects of initial {10-12} twins on cyclic deformation and fatigue of magnesium alloy at low strain amplitudes, Mater. Char. 149 (2019) 118–123.
[43] B. Wen, F. Wang, L. Jin, J. Dong, Fatigue damage development in extruded Mg-3al-Zn magnesium alloy, Mater. Sci. Eng. A 667 (2016) 171–178.
[44] J. Albinmousa, M.J. Adinoyi, N. Merah, Multiaxial fatigue of extruded ZK60 magnesium alloy, Fatigue Fract. Eng. Mater. Struct. 42 (10) (2019) 2276–2289.
[45] L.H. Song, B.L. Wu, L. Zhang, X.H. Du, Y.N. Wang, Y.D. Zhang, C. Esling, Cyclic deformation behaviors of AZ31B magnesium alloy in two different asymmetric loading manners, Mater. Sci. Eng. A 689 (2017) 134–141.
[46] Y. Xiong, Microstructure damage evolution associated with cyclic deformation for extruded AZ31B magnesium alloy, Mater. Sci. Eng. A 675 (2016) 171–180.
[47] S. Dong, Q. Yu, Y. Jiang, J. Dong, F. Wang, L. Jin, W. Ding, Characteristic cyclic plastic deformation in ZK60 magnesium alloy, Int. J. Plast. 91 (2017) 25–47.
[48] A.H. Pahlevanpour, S.B. Behravesh, S. Adibnazari, H. Jahed, Characterization of anisotropic behavior of ZK60 extrusion under stress-control condition and notes on fatigue modeling, Int. J. Fatigue 127 (2019) 101–109.
[49] S. Godet, L. Jiang, A.A. Luo, J.J. Jonas, Use of Schmid factors to select extension twin variants in extruded magnesium alloy, Scr. Mater. 55 (11) (2006) 1055–1058.
[50] J.J. Jonas, S. Mu, T. Al-Samman, G. Gottstein, L. Jiang, E. Martin, The role of strain accommodation during the variant selection of primary twins in magnesium, Acta Mater. 59 (5) (2011) 2046–2056.